OPEN ACCESS

University of BRISTOL

Rose, R. A., Greaves, S. J., & Orr-Ewing, A. J. (2010). Velocity map imaging of the dynamics of reactions of Cl atoms with neopentane and tetramethyl silane. Journal of Chemical Physics, 132, 244312 - 244313. 10.1063/1.3447378

University of Bristol - Explore Bristol Research

General rights

Velocity map imaging the dynamics of the reactions of Cl atoms with neopentane and tetramethylsilane

Rebecca A. Rose, Stuart J. Greaves and Andrew J. Orr-Ewing*

School of Chemistry, University of Bristol, Cantock's Close, Bristol BS8 1TS, UK

13 May 2010

*Author for correspondence

e-mail: a.orr-ewing@bris.ac.uk

tel: +44 117 928 7672

fax: +44 117 925 0612

Abstract

The reactions of ground state $Cl(^2P_{3/2})$ atoms with neopentane and tetramethylsilane have been studied at collision energies of 7.9 ± 2.0 and 8.2 ± 2.0 kcal mol^{-1} respectively. The nascent $HCl(v=0, J)$ products were probed using REMPI spectroscopy combined with velocity map imaging (VMI) to determine rotational level population distributions, differential cross sections (DCSs) and product translational energy distributions. The outcomes from PHOTOLOC and dual-beam methods are compared and are discussed in light of previous studies of the reactions of Cl atoms with other saturated hydrocarbons, including a recent crossed molecular beam and VMI investigation of the reaction of Cl atoms with neopentane [Estillore *et al*. J. Chem. Phys., **132**, 164313 (2010)]. Rotational distributions were observed to be cold, consistent with the reactions proceeding via a transition state with a collinear Cl-H-C moiety. The DCSs for both reactions are forwards peaked, but show scatter across a broad angular range. Interpretation using a model based on linear dependence of scattering angle on impact parameter indicates the probability of reaction is approximately constant across all allowed impact parameters. Product translational energy distributions from dual beam experiments have mean values, expressed as fractions of the total available energy, of 0.67 (Cl + neopentane) and 0.64 (Cl + tetramethylsilane) that are consistent with a kinematic model for the reaction in which translational energy of the reactants is conserved into product translational energy.

1. Introduction

Through extensive experimental and computational studies of the reactions of Cl atoms with a variety of organic molecules, RH (with R denoting alkyl or other classes of organic radical):

$$Cl + RH \rightarrow HCl + R \tag{1}$$

a detailed understanding is emerging of many important characteristics of the dynamics of reactions of polyatomic molecules.[1,2] In addition to numerous measurements of reaction rates,[1] the dynamics of these reactions (and their deuterated analogs) have been examined using a variety of experimental techniques. In an early dynamical study, Flynn and co-workers employed infra-red absorption spectroscopy of the DCl products of reaction of Cl atoms with d_{12}-cyclohexane,[3] but the subsequent combination of resonance enhanced multi-photon ionization (REMPI) or vacuum ultraviolet (VUV) ionization with velocity resolution of reaction products has proved most informative. The velocity information was initially derived from analysis of time-of-flight (TOF) profiles obtained in a TOF mass spectrometer,[4-18] but velocity map imaging (VMI)[19,20] has since become the method of choice.[21-32] The experimental measurements and dynamical calculations for H-atom abstraction reactions involving simple alkanes illustrate a wealth of dynamical behaviour. For example, the shape of the transition state, with near linear Cl-H-C moiety, is reflected in the low rotational excitation of HCl products; scattering angles are largely determined by impact parameter and their distributions can vary with product rotational and vibrational quantum states;[1] and the reactions of Cl atoms with methane and partially deuterated isotopologues exhibit reagent vibrational mode specificity,[4-7,9-12,14,15,33-40] electronically non-adiabatic pathways,[29,31,41,42] and evidence for scattering resonances.[43] Reactions of functionalized organic molecules (RH = alcohols,[24,44,45] amines,[46] alkyl halides[23,47] and linear and cyclic ethers[24,44,48,49]) reveal the effects of weakly bound complexes, molecular reorientation, and molecular shape on the chemical dynamics.[50] The gas phase studies also serve as benchmarks for comparison with recent investigations of the kinetics and dynamics of reactions of the type summarized by (1) (with a variety of organic molecules RH) in liquid solutions using

ultrafast transient absorption measurements of rates of loss of reagents and formation of products.[51-53]

The greatest detail obtained so far from experimental studies of these important polyatomic-molecule reactions comes from VMI measurements of isolated, gas-phase collisions. Here, we use VMI to compare the reactions of Cl atoms with neopentane and tetramethylsilane (TMS):

$$Cl + (CH_3)_4C \rightarrow HCl + (CH_3)_3C(CH_2) \qquad (2)$$

$$Cl + (CH_3)_4Si \rightarrow HCl + (CH_3)_3Si(CH_2) \qquad (3)$$
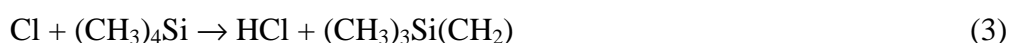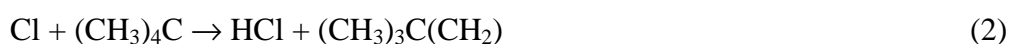
which serve as examples of reactions of large (by the standards of most chemical dynamics studies) polyatomic systems. The organic reagents are chosen because they contain only primary C-H groups, so the complicating effects of competitive reaction at primary and secondary or tertiary sites, with different thermochemistry, are avoided. The experimental data were obtained using both PHOTOLOC[54,55] and dual molecular beam[56] experimental methods, combined in each case with VMI of the HCl products, and comparisons are drawn between the two approaches.

The simplest comparable organic molecule containing only primary C-H groups is ethane (the energetics of the reaction of methane with Cl differ from other alkanes and are thus considered atypical). The dynamics of the reaction:

$$Cl + C_2H_6 \rightarrow C_2H_5 + HCl \qquad (4)$$

have been well studied both experimentally[17,18,22,25-27,45] and computationally,[57-61] and the reactions of Cl atoms with propane[1,62-64] and n-butane[21,25,62] have been similarly investigated. The energetics and kinetics of these reactions are very similar to those for reactions (2) and (3); the reactions are all rapid and direct, have either a low or no barrier to reaction and the exothermicities of the primary hydrogen abstraction reactions are typically about -3 kcal mol^{-1}. They show cold rotational distributions of the HCl products, broad angular scattering and a substantial fraction of the available energy (~20-50%) is deposited into internal energy of the radical coproduct.

There have been a number of studies of the kinetics of reaction of Cl atoms with neopentane which all indicate that it proceeds rapidly, with a low or no activation barrier;[65-69] for example, Kambanis *et al.*[69] determined a temperature independent rate coefficient of 1.1×10^{-10} cm^3 molecule^{-1} s^{-1}. From measurements of the temperature dependence of the rate coefficients for reaction of Cl with TMS, Lazarou *et al.*[70] reported a weak rate enhancement with increasing temperature and deduced an activation barrier of 0.49 ± 0.24 kcal mol^{-1}. The Arrhenius pre-exponential factor for the reaction was determined to be $(3.6 \pm 0.8) \times 10^{-10}$ cm^3 molecule^{-1} s^{-1}, which is close to the hard sphere collision limit at room temperature.

The enthalpy of formation of the $(CH_3)_3SiCH_2$ radical is not precisely known, but the enthalpy change for reaction (3) can be estimated to be $\Delta_r H_0(3) = -3.0 \pm 2.0$ kcal mol^{-1} from a C-H bond strength for TMS of 99.2 kcal mol^{-1} [ref. 71] and an HCl bond strength of 102.2 kcal mol^{-1} [ref. 72,73], with the error limits encompassing the uncertainties in these values. $\Delta_r H_0$ for reaction (2) can be similarly calculated from the C-H bond strength of neopentane. Doncaster and Walsh determined this bond strength to be 0.42 ± 0.17 kcal mol^{-1} greater than in TMS, from which $\Delta_r H_0(2)=-2.6 \pm 2$ kcal mol^{-1} is deduced, and McMillen and Golden[74] reported a C-H bond enthalpy of 100 ± 2 kcal mol^{-1}, implying $\Delta_r H_0(2)=-2.0 \pm 2.0$ kcal mol^{-1}. A $\Delta_r H_0$ value for the Cl + neopentane reaction may also be calculated from the reported enthalpies of formation of the reactants and products,[74-76] giving $\Delta_r H_0(2)=-2.2 \pm 2.0$ kcal mol^{-1}, and a value of $\Delta_r H_0(2)=-2.10$ kcal mol^{-1} was listed by Qian *et al.*[77] Here, we adopt $\Delta_r H_0(2)=-2.5 \pm 2.0$ kcal mol^{-1}, which falls within the specified ranges of all of these values, and with uncertainties reflecting those in the related thermochemical parameters.

The current study presents new data for reaction (2) of Cl with neopentane and extends a previous investigation of the dynamics of reaction (3) of Cl with TMS carried out in our laboratory using the single molecular beam co-expansion method (commonly referred to as the PHOTOLOC technique).[78] In this previous study, REMPI spectra were recorded to determine the nascent rotational populations of the HCl ($v=0,J$) products, and differential cross sections (DCSs) and centre of mass (CM) frame speed distributions were obtained by VMI of the HCl products. The dynamics

of reaction (2) have been the subject of recent investigation by Suits and coworkers using crossed molecular beam (CMB) and VMI methods, with VUV ionization of the hydrocarbon radical product.[79] Here, the dynamics are investigated using both the PHOTOLOC and dual molecular beam methodologies and the results from these two experimental methods, and for the different reactions are compared with each other and the CMB data. The derived rotational, angular scattering and velocity distributions are discussed in light of previous studies of the dynamics of the reactions of Cl atoms with other organic molecules.

2. Experimental

The apparatus used to obtain the results presented has been described in detail elsewhere[31,32] and a brief overview is provided here. It combined UV laser photolysis of Cl_2 as a source of Cl atoms, reaction under low pressure conditions with the neopentane or tetramethylsilane, (2+1) REMPI detection of HCl products, and velocity map imaging onto a 2-dimensional position sensitive detector to record product velocities with rotational and vibrational quantum state specificity. Vacuum was maintained in the reaction and detection chambers by a liquid-nitrogen trapped oil diffusion pump and two turbomolecular pumps.

Two nozzle arrangements were used in the experiments and are illustrated in Figure 1. In the PHOTOLOC experiments samples of Cl_2 (Praxair 99.99%, 20% diluted in Ar) and the organic co-reagent (neopentane, Intergas, 20% diluted in Ar), both at typical backing pressures of 2.5 bar, were expanded into a high-vacuum chamber through separate pulsed nozzles (General Valve Series 9). The two valve orifices were oriented at 90° and the two synchronized gas pulses were merged just prior to expansion into the high vacuum chamber by confining the gas pulses within holes drilled in a PTFE block that intersected at 90° to form a single channel. The merged gas expanded through the repeller plate of the TOF-MS where it was intersected by the counter-propagating and spatially overlapped photolysis and probe (*i.e.*, REMPI) laser pulses.

In the dual molecular beam configuration of the apparatus, the two pulsed nozzles were mounted parallel to one another, with a vertical displacement of their orifices by 17.4 mm. The organic reagent (TMS, Fisher, NMR grade 99.9+%, 75% in Ar; or

neopentane, 75% in Ar) was expanded through the on-axis nozzle which was directed along the centre of the TOF, and Cl_2 (~70% in Ar) was expanded into the vacuum chamber through the other, off-axis nozzle. The Cl_2/Ar expansion was unskimmed and the nozzle was mounted directly to the repeller electrode, whereas the RH/Ar expansion was off-set from the repeller plate by ~12 mm and passed through a 1 mm diameter skimmer. The Cl_2/Ar beam was intersected by the photolysis laser ~ 3 mm from the repeller plate, and the probe laser passed through the RH/Ar molecular beam ~ 6 mm further downstream to compensate for molecular beam speeds so that the most probable CM velocity vectors are in the plane of the imaging detector.[80]

Reaction was initiated by the photolysis of Cl_2 at 355 nm using the third-harmonic of the fundamental output of a pulsed Nd:YAG laser (Continuum Surelite II), operating at 5 Hz, to form >98% $Cl(^2P_{3/2})$ atoms. Product HCl molecules were subsequently probed state selectively by 2+1 REMPI using the two-photon $f^3\Delta - X^1\Sigma^+$ (0,0) transition for resonance enhancement at a one-photon wavelength of ~244 nm. The tunable probe radiation was generated by frequency doubling the output of a dye laser (Lumonics HD 500, Coumarin 480) pumped by 355-nm light from a Nd:YAG laser (Spectra Physics, GCR 230), at a repetition rate of 10 Hz. The time delay settings between the laser pulses are summarised later. The HCl^+ ions were accelerated towards the detector using extraction electric fields and projected onto the detector after passage through a field-free TOF region. The extraction fields could be configured for DC slice-imaging, or, if total ion signals were required, for conventional VMI. The detector consisted of a pair of 75-mm diameter microchannel plates (MCPs) and a phosphor screen. Light emitted from the phosphor screen as a result of impacts by ions on the MCPs was observed by a photomultiplier tube (PMT) and a CCD camera, with the latter providing spatial information on the points of impact. The observed raw images for both the PHOTOLOC and dual beam methods showed good circularity and left-right symmetry (as well as up-down symmetry for PHOTOLOC. data). The dual-beam images were, however, left-right symmetrized prior to analysis to improve signal-to-noise ratios.

3. Results

Three different sets of experimental measurements are presented here. First, the populations of different rotational quantum states of the HCl reaction products are

reported, followed by velocity map images for selected HCl ro-vibrational quantum states obtained using the PHOTOLOC and the dual molecular beam configurations of the apparatus. Under the experimental conditions, with photoinitiation by 355-nm photolysis of Cl_2, the mean collision energies for the Cl atom reactions with neopentane and TMS are 7.9 and 8.2 kcal mol^{-1} with estimated variation about the mean of $\pm$ 2 kcal mol^{-1} resulting from thermal motion of the Cl_2 and RH molecules.

3.1 Rotational distributions

For experimental measurements of populations of the HCl rotational levels, the single molecular beam late mixing nozzle configuration was used in combination with standard imaging voltages on the ion optics to generate a 2D projection of the 3D velocity distribution. REMPI spectra of the HCl products of reaction (2) were obtained by scanning the wavelength of the probe laser and recording the total ion yield at the detector for the mass-to-charge ratio m/z=36. Figure 2(a) shows representative spectra, and the assignments of the spectral lines are indicated. Equivalent data for reaction (3) have been presented previously.[78] These experiments are prone to low, but detectable, levels of HCl contamination from the Cl_2/Ar gas line. This background signal is independent of the photolysis laser and can be removed using a shot-to-shot subtraction procedure to extract nascent reactive signals which depend on the presence of both the photolysis and the probe lasers. This background subtraction procedure is demonstrated in Figure 2(a).

Five sets of spectra were taken over the Q, R and S- branch lines indicated in Figure 2(a). The spectra were converted into nascent relative populations of the HCl(v=0, *J*) rotational levels using previously published correction factors[45] to convert from integrated areas of the lines. The normalised distributions of the rotational populations are plotted in Figure 2(b), where they are compared to results from prior measurements for the reaction of Cl atoms with ethane[45] and tetramethylsilane.[78] The errors indicated in Figure 2(b) include 1 standard deviation (s.d.) uncertainty in multiple replicate measurements and uncertainties in the correction factors. The rotational distributions show that in all cases HCl is formed predominantly in low rotational levels (*J*=0-3), with populations peaking at *J*=1 for the reactions of Cl atoms with ethane and neopentane and *J*=2 for the reaction with TMS. From a Boltzmann plot of the rotational populations for the reaction of Cl atoms with

neopentane a value for the rotational temperature of 82 ± 5 K was derived. This can be compared to rotational temperatures of 117 ± 5 K and 123 ± 6 K deduced previously for the reactions of Cl atoms with ethane[45] and TMS,[78] respectively.

3.2 Cl + neopentane PHOTOLOC imaging

In this section, velocity map images for reaction (2) are presented for the late-mixing, single molecular beam co-expansion configuration shown in Figure 1. The low rotational excitation of the HCl products of the reaction reported in the preceding section limited velocity map images to HCl(v=0,J) with J=0-2. Images were accumulated over ~60000 laser shots, with a fixed time delay of 50 ns between the photolysis and probe laser pulses. The probe laser wavelength was scanned back and forth across the full Doppler width of the HCl REMPI transition during image accumulation to avoid bias towards a particular velocity subset of products. Images were accumulated in separate buffers on an alternate shot-to-shot basis for both lasers firing, and for the photolysis laser off, and images were obtained by subtraction of a background image from an image obtained with both lasers on. The images were analysed using the Legendre moment method of Brouard and co-workers.[21,22] Figure 3 shows a representative image for HCl(v=0,J=0) obtained from reaction (2), together with the derived lab frame speed (v_p) dependent zeroth- and second order Legendre moments of the image, $L_0(v_p)$ and $L_2(v_p)$, respectively. The Legendre moments of the image can be related to lab frame speed, P(v_p) and speed dependent anisotropy distributions, $\beta(v_p)$, by:[22] P(v_p)=$v_p L_0(v_p)$ and $\beta(v_p)$=$L_2(v_p)/L_0(v_p)$. Figure 3 also shows fits to both these distributions.

Figure 4 shows the outcomes of fits to the Legendre moments of the image in Figure 3 using basis functions constructed from various numbers of Legendre polynomials used to expand the speed and angular functions. Inputs to the fits include the velocity distribution of the Cl atom photofragment (obtained from images of the photodissociation of Cl_2 at 355 nm) and the energy released in the reaction. Basis functions for the reaction were calculated from this input information and consisted of separable expansions of Legendre moments in $\cos\theta$, where θ is the CM frame scattering angle and f_t'=2f_t-1, where f_t is the fraction of available energy which transforms into product translational energy release. From fits to the experimental Legendre moments, the CM-frame angular distribution (the DCS) and f_t distribution,

P(f_t) were determined. The numbers of Legendre polynomials used in the expansions of the angular and f_t' distributions can be varied independently and the notation (n,m) denotes the respective numbers employed. Figures 4(a) and (b) show the f_t and DCS distributions that result from the fits of the (3,3), (3,5) and (4,4) Legendre polynomials to the Legendre moments of the image shown in Figure 3. The f_t distributions peak at f_t =1.0 in all cases, but become more oscillatory as the number of Legendre polynomials in f_t' increases. The oscillatory forms are an artefact of too many basis functions in the fit, but the mean f_t derived from each of these distributions, $\langle f_t \rangle$ =0.74±0.02, is independent of the number of Legendre moments used in the fitting procedure. The uncertainty is 1 s.d. in the values derived from the different analyses. The fits shown in Figure 3 capture the main form of the lab frame speed distribution, but are poorer at the high lab frame speed end of the distributions. This may reflect an underestimate of the reaction enthalpy, which would force the fits towards larger f_t in the P(f_t) distributions. Use of alternative Legendre moment basis functions generated with an exothermicity of $\Delta_r H_0$ = -5 kcal mol^{-1} improved the quality of the fits at high lab frame speed. The resulting DCS is very similar to that shown in Figure 4, but the mean f_t shifts to a lower value of 0.65 in accord with the increase in energy available to products.

Similar analysis of the lab frame speed dependent zeroth- and second-order Legendre moments from images of HCl(v=0, J=1 and 2) products was carried out. Panels (c) and (d) of Figure 4 compare the f_t distributions and DCSs for the J=0-2 products derived from fits with (4,4) sets of Legendre polynomials. The error bars in the DCSs indicate the uncertainties in the fits derived from using different numbers of Legendre polynomials and from replicate images. The derived P(f_t) and DCS are observed to be independent of the rotational state of HCl, and the DCSs show broad but predominantly forwards scattered distributions (defined with respect to the Cl atom velocity). Mean values of f_t of 0.73 ± 0.03 and 0.74 ± 0.03 are derived for J=1 and 2 respectively, and are within the uncertainty of the value derived for J=0.

Data previously recorded for the Cl + TMS reaction using the PHOTOLOC method[78] were reanalysed because of recognition that the $\beta(v_p)$ data were affected by a residual background signal and so underestimated the spatial anisotropy at larger v_p values. The $\beta(v_p)$ distributions were therefore given no weight in the revised fitting

procedure. In contrast to the results of the prior analysis, the outcomes of these fits show angular scattering that is broadly similar to the results presented for the Cl + neopentane reaction, with more forward than backward and sideways scatter and $\langle f_t \rangle \sim 0.50$.

3.3 Dual beam imaging

Experiments conducted with the dual molecular beam configuration illustrated in Figure 1 required the background subtraction and Doppler scanning methods described in the preceding section, but also necessitated stepping of the time-interval between the two laser pulses. The photolysis laser preceded the probe laser by intervals of 9.5 – 16.0 μs, and the delay was increased from the minimum to the maximum value in steps of 250 ns as images were accumulated. The variation of the time interval between the lasers minimises any bias in the experiments between the detection of faster or slower moving products; the former tend to result from forwards scattering in the CM frame, and the latter from backwards scattering.[25]

Velocity map images for HCl(v=0,J=0-3) from reactions of Cl with neopentane and TMS are shown respectively in Figures 5 and 6. The displayed images have undergone the background subtraction procedure, and have been symmetrised about the central vertical axis. In the images, the average relative velocity vector (v_{rel}) and the velocity of the centre of mass (u_{CM}) lie in the vertical direction, along the central symmetry axis, as indicated in the inset Newton diagrams. These Newton diagrams are constructed from u_{CM} and the CM-frame HCl product velocity, u_{HCl}, for each reaction. The mean CM velocity for the reaction of Cl atoms with neopentane is 550 ms^{-1} and the maximum energetically available CM-frame speed for HCl products with no rotational excitation is 1265 ms^{-1}. For the reaction of Cl atoms with TMS the corresponding CM and maximum product speeds are 475 ms^{-1} and 1370 ms^{-1}. Forward and backward scattered HCl products are observed in the upper and lower hemispheres, respectively. Also shown in the Figures are the angular distributions (integrated over all speeds), I(θ), and the speed distributions (integrated over all scattering angles), P(v), which are derived from the radial dependence of the images. The conversion from radial distance in an image to speed was performed using a linear conversion factor obtained from images of the photodissociation of Cl$_2$. As has been shown previously,[24,80] the angular dependence should be an almost direct

11

measure of the CM-frame DCS. Within the uncertainties in the derived angular distributions, the outcomes are identical for HCl(v=0,J) for J = 0-3 for each of the reactions, and are the same for the products of the two reactions. The distributions of f_t peak at ~0.80 and ~0.75 for the reactions of Cl atoms with neopentane and TMS, respectively and Table 1 summarises the mean values of f_t for the HCl(v=0,J) reaction products. The errors given in the table arise primarily from the 2 kcal mol^{-1} uncertainties in the enthalpies of both of the reactions, but also encompass errors in the reproducibility of the measurements, which are not more than ±4%. The mean values of f_t are independent of J for each reaction and are the same within experimental error for the two reactions.

In a recent study of the dynamics of the CH_3 + HCl reaction using the dual molecular beam methodology, we reported an under-detection of products scattered downwards in the laboratory frame (corresponding to backwards scattering in the current experiments). This under-detection was attributed to depletion of the products that scatter in directions opposed to the velocity of the centre of mass, and which thus have slower laboratory frame speeds. The depletion is most likely to be a result of these products spending a longer time in the region of the upper, on-axis molecular beam and thus undergo secondary collisions that deflect them away from the volume sampled by the probe laser beam. The same depletion is evident in the images and angular distributions displayed in Figures 5 and 6 and we have developed two alternative methods to correct for the under-detection of the backwards scattered products. The first method uses a calibration reaction for which the DCS is known from CMB experiments,[26,27] and the second is to use the outcomes of a comprehensive Monte-Carlo (MC) simulation of the experiments that is similar in spirit to the approach used by Suits and coworkers for a related experimental design.[80] In both cases an angular correction function is generated, and the two are similar in form and magnitude. The details of the first method have been described elsewhere,[32] but, in brief, an experimental angular correction function was obtained by comparison of dual molecular beam images for reaction (4) with CMB and VMI results reported by Huang *et al*.[27] at a similar collision energy.

The MC simulations used to derive an alternative angular correction function incorporate the velocity distribution of the Cl atom reagent, the reaction energetics

and many further features of the experiment, including the divergence and speed of the molecular beams, the geometry of the experiment and the volumes of the photolysis and probe lasers. Parameters in the computer code describing these various experimental features were determined by extensive characterization of the apparatus. A user-defined input DCS employed in the simulations was selected to be uniform in $\cos\theta$ and ϕ (i.e. spherically uniform) and images were simulated for f_t = 0.01-0.99 in steps of 0.01 and then summed. The MC simulations confirm the need to step over a range of time delays between the photolysis and probe lasers to weight correctly the detection of products scattered into the forward and backward hemispheres.[25] Thus, simulated images are summed over selected time delays from 9.5 – 16.0 μs, in accord with the acquisition of experimental images. The simulations assume a (secondary) collision probability for the HCl products of the reaction that depends exponentially on the time spent within the volume swept out by the RH/Ar molecular beam, as can be justified from a model of pseudo-first order collision kinetics. The angular correction function generated has the form $[f_{sim}/\exp(a)]\exp(at_{HCl}/t_{HCl}^{min})$ with $a = 1.55$ (a value that can be understood in terms of the number density in the molecular beam and an assumption of gas-kinetic collision rates) which quantitatively reproduces the experimentally derived correction function. Here, f_{sim} is a correction factor derived from the MC simulation program with the neglect of secondary collisions, the exponential term accounts for the effects of secondary collisions and t_{HCl} is the average time HCl spends in the RH molecular beam as a function of scattering angle (scaled by the average minimum time t_{HCl}^{min} ~1.5 μs).

The correction functions derived for the Cl + neopentane and Cl + TMS reactions are shown in Figure 7. The simulated f_t distribution, P(f_t) reported in the Figure is for scattering angles from 0-120°, corresponding to the region in which the majority of the experimental signal is observed. The simulations show a bias against the detection of HCl products formed with the highest kinetic energy release. This is similar to the bias reported for simulations of the Cl + ethane and CH_3 + HCl reactions[32] and was attributed to the effect of a spread in product speeds combined with a lower detection efficiency for high f_t products. After correction for the computed bias in the f_t distribution, mean values of f_t of 0.67 and 0.64 are derived for the reactions of Cl with neopentane and TMS respectively.

The distributions reported as a function of angle are for images summed over f_t=0.4-0.99, the range in which the majority of the signal is observed experimentally. Angular correction factors for reactions (2) and (3) derived from the MC simulations are shown in the bottom panel of Figure 7. These correction factors employed the functional form described above. Angular distributions obtained by correction of the data plotted in Figure 5 and Figure 6 using the correction functions derived from both the MC simulations and empirically from measurements on the $Cl + C_2H_6$ reaction are displayed in Figure 8. As noted above, the angular distributions derived directly from the images are independent of J, therefore the data in Figure 8 are obtained from rotational population weighted averages of the angular data in Figure 5 and Figure 6 for the reaction of Cl atoms with neopentane and TMS respectively. The data corrected by the experimentally determined function are curtailed at a scattering angle of 150° because the angular correction function did not extend further into the backward scattering direction. For both reactions, the corrected angular distributions are forward peaking but extend across all scattering angles, consistent with the results of the PHOTOLOC experiments described in section 3.2. The DCSs derived by correction from the two different methods are broadly in agreement for both reactions; the agreement is almost perfect between 0 and 60º where the corrections are small (both correction factors are close to unity), but the differences become larger as the scattering angle increases. It can also be noted that the majority of signal is observed in the images at scattering angle less than 60º and only weak scattering is observed into angles greater than 90º; uncertainties in the DCS after correction are necessarily higher for backwards scattered products because of a combination of these low signal levels and uncertainties in the form of the correction function. The error bars plotted in Figure 8 reflect both these effects.

The validity of use of the angular correction functions employed to give the DCSs plotted in Figure 8 can be tested by using the derived angular and speed distributions in the CM frame to simulate the expected forms of the data obtained from a PHOTOLOC and VMI experiment. The raw data obtained from the single molecular beam experiments were therefore simulated using the dual-beam results by inversion of the standard equations used for PHOTOLOC analysis.[54,55] In Figure 9, the speed and anisotropy data obtained for the single-beam experiments for reaction (2) are

compared with simulations derived from the P(v) distributions plotted in Figure 5 and the two forms of the DCS plotted in Figure 8. The simulated PHOTOLOC data obtained using the DCS derived from correction of the angular distributions using the MC simulated function show good agreement with the raw experimental data. The agreement is less good between the experimental data and the simulated PHOTOLOC data using the DCS derived from application of the experimentally determined angular correction function (extrapolated to 180°), particularly in the region of slower lab frame products. This suggests that this correction function over-estimates the population of backwards scattered products. In both simulations, the proportion of products formed with a lab frame velocity of ~1000 ms^{-1} is underestimated (see later). The otherwise good agreement between the experimental and simulated PHOTOLOC data lends support to the correction of the angular distributions from the dual beam experiments using the correction function derived from MC simulations.

4. Discussion

4.1 Rotational distributions

Many features of the dynamics observed for the Cl + neopentane and Cl + TMS reaction are similar to those reported for the reactions of Cl atoms with small alkanes other than methane, which, as noted previously, is atypical. Cold rotational distributions are commonly observed for these reactions which proceed via a transition state where the Cl-H-C moiety is nearly collinear, followed by negligible interaction between the departing products in the exit channel of the PES.[1,3,18,21,62] The transition state for the Cl + neopentane reaction and neopentyl radical structures were computed at the B3LYP/aug-cc-pvdz level of theory;[81] the outcomes of the calculations are compared to previously calculated structures for the reactions of Cl atoms with ethane[57] and TMS[78] in table 2. The Cl-H-C bond angle is close to linear in all cases, thus little torque is imparted on the departing HCl product. The computed dipole moments of the organic radical products are small, so interactions between the departing species are expected to be weak. Both of these factors are consistent with the low rotational temperature of the HCl products observed experimentally.

Valentini and coworkers[82] proposed a kinematic model for reactions such as (1-3) which involve the transfer of a light atom between two heavier centres. Within this model, restrictions are imposed on the maximum rotational angular momentum of the

product HCl. This model has been found to work well for the reactions of Cl atoms with small hydrocarbons; for example Kandel et $al.$[18] observed a maximum populated rotational level of J=8 for the Cl+C_2H_6 reaction, which is close to the maximum of J=9 predicted by the model. Using this kinematic model, the highest rotational level populated is calculated to be J=10 for the reaction of Cl atoms with neopentane and TMS, which is greater than the J=4 or 5 limit observed within the signal to noise limit of our experiments. Kinematic constraints thus do not appear to be the limiting factor in the rotational energy disposal to HCl; instead the low rotational excitation is proposed to result from the TS structure and the weak post-TS interactions.

4.2 Internal excitation of the radical products

For the reactions of Cl atoms with either neopentane or TMS, significant internal excitation of the radical coproduct was deduced from the product speed distributions. The dual molecular beam experiments (after MC correction for biases in the f_t distributions) suggest that ~33-36% of the total energy available to products ends up in the internal excitation of the neopentyl or tetramethylsilyl radical, whereas in the co-expansion experiments the value is ~26% for the Cl + neopentane reaction. The PHOTOLOC fits maximise at f_t=1 because of the need to fit to fastest lab speeds which extend up to and beyond the maximum speed expected from the estimated energetics of the reaction discussed in the Introduction. The discrepancies between the derived values of the internal excitation of the radical coproduct from the two experimental methods are significant, but similar discrepancies have been noted for the reaction of Cl atoms with ethane,[22,25,27] and for the CH_3 + HCl reaction[32] when comparing the results of dual or crossed molecular beam experiments with the results of PHOTOLOC experiments.

In recent crossed molecular beam VMI experiments on the Cl + neopentane reaction at a collision energy of 8.0 kcal mol^{-1}, Suits and coworkers probed the neopentyl radical product by single photon ionisation at 157 nm and deduced product angular and translational energy distributions.[79] The mean translational energy release was shown to decrease as the scattering angle increased and similar behaviour was observed by Huang et $al.$ for the Cl + ethane reaction.[27] The analysis employed for our PHOTOLOC data treats the product angular and translational energy distributions as independent. In principle our images obtained using the dual molecular beam method

measure product velocities in the CM frame, but as was discussed earlier, suffer from undercounting of signal in the backward ($\theta = 120\text{-}180°$) and, to a lesser extent, sideways ($\theta = 60\text{-}120°$) directions, which prevents determination of correlated angular and f_t distributions. The mean f_t values derived in our experiments are slightly higher than the values of 0.54 and 0.56 deduced by Suits and coworkers for averaging over all angles, and for products scattered into the forwards direction ($\theta = 0\text{-}60°$) respectively.

The degrees of internal excitation of the radical products are comparable in magnitude to the values derived from studies of other Cl + alkane reactions. In PHOTOLOC experiments combined with Legendre moment analysis for the reactions of Cl atoms with ethane and n-butane at collision energies of 5.5 and 7.4 kcal mol^{-1}, Brouard and coworkers deduced that the internal excitation of the radical product was, respectively, ~22% and ~ 30%.[21,22] In CMB studies of the Cl + propane reaction, Blank et al.[63] showed that ~40-50% of the available energy was channelled into internal excitation of the propyl radical. Huang et al.[27] used CMB methods to investigate the Cl + ethane reaction at four collision energies between 3.2 and 10.4 kcal mol^{-1} and found that f_t for forward scattered products decreased as the collision energy increased, but the absolute internal energy of the ethyl radicals remained almost constant at ~3 kcal mol^{-1}, which is close to the exothermicity of the reaction. Thus, as the collision energy increases, the additional translational energy of the reactants is transformed into the translational energy of the products, consistent with a kinematic model for a light atom abstraction reaction which decouples the internal and translational degrees of freedom.[27,82] A similar kinematic model for the Cl + TMS and Cl + neopentane reactions at the collision energies used here leads to an expectation of ~30% internal excitation of the radical co-products, which is within the uncertainties of the values derived from data in Table 1.

The internal excitation of the neopentyl and tetramethylsilyl products may reside in rotational and/or vibrational degrees of freedom, but experimental studies which probe the HCl products give no information on which degrees of freedom are excited. The change in geometry from tetrahedral to planar around the carbon atom from which the H atom is abstracted might be expected to induce vibrational excitation.

However, as is evident from table 2, the calculated transition states for the reactions of Cl atoms with ethane, neopentane and TMS are product-like, with r_{C-H} greater than r_{Cl-H}, so the TS occurs late in the reaction path. This might reduce the tendency towards vibrational excitation of the products.[83] In *ab initio* trajectory studies of the reaction of Cl + C_2H_6, Rudić *et al.*[57] found that the internal energy of the ethyl fragment was mostly accounted for by rotational excitation, which is induced by the torque imparted about the ethyl centre-of-mass as the reaction products separate from the transition state. A similar mechanism can be proposed for the reactions of Cl atoms with neopentane and TMS, thus a substantial fraction of the internal excitation might be expected to reside in the rotational modes of the radical, although we note that the neopentyl radical has many low frequency vibrational modes that could accommodate the internal energy

4.3 Centre of mass frame angular scattering

The DCSs derived from PHOTOLOC and dual molecular experiments for the reactions of Cl atoms with neopentane are compared in Figure 10, and are in good agreement, although the PHOTOLOC results show greater scattering into the sideways directions. This difference is consistent with the discrepancies observed in Figure 9 at lab speeds around 1000 m/s and may stem from uncertainties in the angular correction function applied to the dual molecular beam data, or because of assumptions made in the PHOTOLOC analysis such as the seperability of angular and speed distributions. Figure 8 shows that the product scattering derived from dual molecular beam experiments for the reactions of Cl atoms with neopentane and TMS are the same within experimental error. In both cases, scattering across all angles is observed, with enhanced flux into the forwards direction. Similar scattering distributions are observed for the reaction of Cl atoms with other small saturated hydrocarbons. The results of crossed molecular beam experiments on the Cl + neopentane reaction conducted by Suits and coworkers[79] are plotted in Figure 10 for comparison with our data. The DCSs are broadly similar, but our results are less sharply peaked in the forwards direction, and show reduced backward scattering. The DCS for the reaction of Cl atoms with ethane reported by Huang *et al.*[27] at the higher collision energy of 10.4 kcal mol^{-1} is also shown in the Figure because of its remarkable similarity to the outcomes of our measurements for reactions of neopentane and TMS. Good agreement is also seen with the DCSs derived by Brouard and coworkers[21] for the HCl(v=0, J=0 and 3) from

18

the primary hydrogen abstraction channel of the Cl + n-butane reaction at a comparable collision energy of 7.4 kcal mol^{-1}. The DCSs presented for the HCl(v=0,J =0-3) products of the reactions of Cl atoms with neopentane and TMS show no dependence on J. By way of comparison, the previously reported DCSs for HCl(v=0,J =0-8) from the reaction of Cl atoms with ethane do exhibit some J dependence,[17,18,22,25-27] but with little variation for J = 0 - 3.

The broad scattering is often ascribed to a wide cone of acceptance, resulting from a loose transition state, so that the approach of the Cl atom is not tightly constrained,[1] and greater product scattering in the forward direction tends to be observed as the collision energy increases.[27] A simple hard sphere model predicts the relationship between the product scattering angle, θ, and the impact parameter, b, of a collision to be:[5]

$$\cos\theta = \frac{2b^2}{d^2} - 1 \tag{5}$$

where b defines the radial distance between the centres of mass of the colliding species and d is the sum of the radii of the reactants. This gives rise to the following form of the DCS:

$$\frac{d\sigma}{d\cos\theta} = \frac{\pi d^2 P(b)}{2}, \tag{6}$$

where $P(b)$ is the opacity function which describes the probability of reaction at a given impact parameter. From Eq. (6) the forms of the opacity function for the reactions of Cl atoms with neopentane and TMS can be derived, and the outcome (deduced to be the same for both reactions) is shown in Figure 11(a). The shaded region encompasses the range in the opacity function from analysis of different data sets from dual molecular beam and co-expansion experiments. $P(b)$ peaks at the maximum impact parameter, b_{max} so has been scaled to a value of 1 at b/b_{max}=1, which corresponds to a scattering angle of 0°. The opacity function shows that reaction occurs across all impact parameters, but suggests that a stripping mechanism with peripheral dynamics dominates.

Fully dimensional quasi-classical trajectory (QCT) calculations of the reaction of Cl atoms with ethane,[59] showed that the relationship in Eq. (5) did not apply well, however, and therefore the scattering could not be described simply by a hard sphere model for collisions. This will be because the true PES for the reaction deviates from the purely repulsive step function that describes the hard sphere potential. The impact parameter was instead found to be approximately linearly correlated with the scattering angle. Using this correlation, an alternative relationship between the DCS and the opacity function can be derived (as is outlined in the Appendix):

$$\frac{d\sigma_r}{d\cos\theta} = \frac{2b_{max}^2}{\pi\sin\theta}(\pi-\theta)P(b) \tag{7}$$

The resulting opacity function for the reactions of Cl atoms with neopentane and TMS is shown in Figure 11(b), with the uncertainty resulting from different experimental DCSs indicated by the shaded region. Within this model the reaction can no longer be described as being dominated by a stripping mechanism; the form of the opacity function suggests that reaction occurs across all impact parameters approximately equally, or with small impact parameter collisions weakly favoured.

5. Conclusions

Velocity map imaging and REMPI spectroscopy have been applied to study the dynamics of the reactions of Cl atoms with neopentane and tetramethylsilane. The nascent HCl(v=0,J) products of the Cl + neopentane reaction were found to be formed rotationally cold with a distribution of rotational states which is similar to those measured previously for the reactions of Cl atoms with ethane and TMS. Such cold rotational distributions are consistent with the computed near linear transition states for these reactions. The CM frame scattering distributions of the HCl(v=0,J=0-3) products of the reactions of Cl atoms with neopentane and TMS were derived using the dual molecular beam method. These results were compared to the DCSs for the HCl(v=0, J=0-2) products of the Cl + neopentane reaction determined using the PHOTOLOC method and previous PHOTOLOC measurements of the scattering of the HCl products of the Cl + TMS reaction (corrected from a previous analysis). The

DCSs derived from the different methods are broadly consistent and show that, within experimental error, the DCSs for the different rotational states of HCl and for the two different reactions are the same. The CM angular distributions show broad but predominantly forwards scattered distributions which are very similar to those observed for the reactions of Cl atoms with ethane and butane. Such distributions can be interpreted in terms of a wide cone of acceptance for a loosely constrained transition state which allows reaction over large range of impact parameters. Within a simple hard sphere and line of centres model for the reactions, the preponderance of forwards scattered products implies a peripheral mechanism where high impact parameter collisions dominate. However, an alternative model is proposed in line with the results of QCT calculations of Greaves *et al.*,[59] which suggests reactivity is close to uniform across all impact parameters. Significant (~35% of the available energy) internal excitation of the neopentyl and tetramethylsilyl radicals is consistent with kinematic constraints for light atom abstraction reactions which require translational energy of the reactants to be conserved in the products. In line with the QCT calculations by Rudić *et al.*[57] for the Cl + ethane reaction, much of the internal energy of the radicals can be proposed to reside in rotational modes.

Appendix

In quasi-classical trajectory calculations of the reaction between Cl atoms and ethane, Greaves *et al.*[59] showed that the impact parameter, b, is linearly related to the product scattering angle, θ, with collisions at large impact parameters leading to forwards scattered products, and small impact parameter collisions resulting in backwards scattered products. The QCT calculations exhibit the relationship:

$$b = b_{max}\left(1 - \frac{\theta}{\pi}\right).$$
(A1)

The integral cross section is linked to the differential cross sections with respect to b and $\cos\theta$ by:[84]

$$\sigma_r = \int_0^{b_{max}} \frac{d\sigma_r}{db} db = \int_{-1}^{1} \frac{d\sigma_r}{d\cos\theta} d\cos\theta$$
(A2)

Here,

$$\frac{d\sigma_r}{db} = 2\pi b P(b) \qquad\qquad (A3)$$

where $P(b)$ is the opacity function which describes the probability of a reaction at an impact parameter b. Using equation (A3) with an expression for $db/d\theta$ from (A1) gives:

$$\frac{d\sigma_r}{d\theta} = \frac{b_{max}}{\pi}.2\pi b P(b) \qquad\qquad (A4)$$

The differential cross section with respect to $\cos\theta$ can therefore be written as:

$$\frac{d\sigma_r}{d\cos\theta} = \frac{d\sigma_r}{\sin\theta d\theta} = \frac{2bb_{max}P(b)}{\sin\theta} \qquad\qquad (A5)$$

Substituting Eq. (A1) into Eq (A5) gives an expression linking the opacity function to the DCS:

$$\frac{d\sigma_r}{d\cos\theta} = \frac{2b_{max}^2}{\pi\sin\theta}(\pi-\theta)P(b) \qquad\qquad (A6)$$

providing us with a preprint of their paper on the reactions of Cl atoms with pentane isomers, and for the crossed molecular beam data plotted in Figure 10.

Table 1: The rotational state dependent fraction $\langle f_t \rangle$ of the available energy released as translational energy for HCl(v=0,J) products of the reactions of Cl atoms with neopentane and TMS. The values assume reaction enthalpy changes of -2.5 kcal mol^{-1} and -3.0 kcal mol^{-1} respectively. Error ranges result primarily from the uncertainties in the reaction enthalpies but also encompass 1 s.d. in the values derived from 3-5 different images. The average values of $\langle f_t \rangle$ across all rotational states are specified before and after correction by the Monte-Carlo computed bias in the f_t distributions, as described in the text.

J	$\langle f_t \rangle$	
	Neopentane	Tetramethylsilane
0	0.63 ± 0.12	0.59 ± 0.12
1	0.64 ± 0.12	0.59 ± 0.12
2	0.64 ± 0.12	0.58 ± 0.12
3	0.64 ± 0.12	0.57 ± 0.12
Average	0.64 ± 0.12	0.59 ± 0.12
Corrected	0.67 ± 0.12	0.64 ± 0.12

Table 2: Computed transition state (TS) Cl-C-H angle and C-H (for the reactive bond) and Cl-H bond lengths, and product radical dipole moments for the Cl + RH → HCl + R reaction, with RH = ethane,[57] neopentane or TMS.[78] For the reactions with neopentane and TMS the TSs and radical properties are computed at the B3LYP/aug-cc-pvdz level of theory and for the reaction with ethane at the MP2/6-311G(d,p) level of theory.

	Ethane[57]	Neopentane	TMS[78]
$\angle$Cl-H-C / °	177	178	176
r_{C-H} / Å	1.46	1.7	1.6
r_{Cl-H} / Å	1.35	1.4	1.4
μ(radical) / D	0.27	0.29	0.05

Figure 1: Schematic diagram of the VMI experimental setup. The insets to the left show the configurations of the nozzles in the dual (top) and single (bottom) molecular beam experiments. R is the repeller electrode, L_1 and L_2 are two lens electrodes and G is a grounded electrode.

Figure 2: (a) 2+1 REMPI spectra of parts of the R, S and Q-branches of the $f^3\Delta_2$-$X^1\Sigma^+(0,0)$ transition of the nascent HCl($v=0,J$) products of the reaction of Cl atoms with neopentane and (b) the derived rotational level populations, P(J), for HCl($v=0,J$) products of the reaction of Cl + C(CH$_3$)$_4$ (triangles) compared to the rotational populations derived for the reaction of Cl atoms with C$_2$H$_6$ (open squares)[45] and Si(CH$_3$)$_4$ (circles).[78] In (a) the two color (355 nm laser on; solid line), probe only (355 nm laser off; dashed line) and background subtracted difference signals (lower solid line) are plotted and have been vertically off-set for clarity.

Figure 3: Lab-frame speed dependent zeroth- and second- order experimental Legendre moments ($L_0(v_p)$ and $L_2(v_p)$, respectively) of the DC slice image (inset) of the HCl($v=0,J=0$) products of the Cl + neopentane reaction (solid lines). The dashed lines show the best fits obtained using the Legendre moment fitting procedure with (4,4) Legendre polynomials in cos θ and f_t'. Fits with (3,3) and (3,5) sets of Legendre moments were almost indistinguishable from the (4,4) fit shown.

Figure 4: Centre of mass frame f_t distributions, P(f_t), and DCSs, dσ/dcosθ, resulting from fits to the lab frame speed and anisotropy data shown in Figure 3. Panels (a) and (b) show the f_t distributions and DCSs respectively resulting from fits of (3,3) (fine solid line), (3,5) (dotted line) and (4,4) (thick solid line) combinations of Legendre moment basis functions to the data in Figure 3. Panels (c) and (d) compare f_t distributions and DCSs resulting from the (4,4) Legendre polynomial fits for $J=0$ (solid), $J=1$ (dotted) and $J=2$ (dashed) rotational levels of HCl. The uncertainties shown for the DCS for HCl($v=0,J=0$) products encompass errors from the differences in the DCSs derived from fitting with different numbers of Legendre moments and the variations from fits to replicate images; errors in the DCSs for the other rotational levels are comparable in magnitude. Uncertainties in P(f_t) are discussed in the text.

Figure 5: Velocity map images of the HCl(v=0, J=0-3) products of the Cl + neopentane reaction and the derived speed and angular distributions. The Newton diagram for the reaction is shown at the top. Images have been symmetrised along the central vertical axis which is parallel to the average centre-of-mass vector. The distributions are the average of 3-5 data sets and the uncertainties indicated are 1 s.d. in the data.

Figure 6: As for Figure 5, but for the Cl + TMS reaction. Velocity map images are shown for the HCl(v=0, J=0-3) products of the Cl + TMS reaction, together with the derived speed and angular distributions.

Figure 7: Outcomes of Monte Carlo simulations of experimental performance for the reactions of Cl atoms with neopentane (left) and TMS (right). Top: the fractional translational energy release; middle: the angular scattering distributions, with neglect of secondary collisions; and bottom: the full angular correction function incorporating a model for secondary collisions. The f_t and angular distributions input into the simulation program are displayed as dashed lines in the top two plots.

Figure 8: Differential cross sections for the reaction of Cl atoms with (a) neopentane and (b) TMS. The DCSs are derived from the angular distributions presented in Figures 5 and 6 multiplied by either the experimental (dashed line) or MC-simulated (solid line) angular correction functions.

Figure 9: Comparison of experimental (grey circles) PHOTOLOC distributions for the Cl + neopentane reaction with simulations (black lines) based on dual-beam experimental results. The top panel shows lab frame speed distributions and the bottom shows the speed-dependent anisotropy. Two simulations are compared: for both, the input CM frame speed distribution is derived from an average of the data presented in Figure 5, and CM angular distributions are either the experimentally (dashed line) or MC corrected (solid line) angular distributions presented in Figure 8. See text for further details.

Figure 10: Comparison of the DCSs for the Cl + neopentane reaction derived from dual molecular beam experiments (solid black line) and co-expansion experiments

(dashed black line; as in Figure 4(d)) at a collision energy of 7.9 kcal mol^{-1}. The DCSs obtained from the crossed molecular beam experiments of Suits and coworkers for the Cl + neopentane reaction[79] at a collision energy of 8.0 kcal mol^{-1} (solid grey line) and the HCl(v=0,J=2) products of the Cl + ethane[27] reaction (dashed grey line) at a collision energy of 10.4 kcal mol^{-1} are also plotted. Dual beam data are the mean of the two data sets presented in Figure 8(a) for the Cl + neopentane reaction and have undergone 3 point adjacent averaging to smooth the data. The error bars encompass uncertainties in the experimental measurements and in the correction of the data.

Figure 11: Opacity functions generated from (a) a hard sphere and line of centres model for scattering and (b) an alternative model described in the text. The shaded area in both cases represents the uncertainty in the opacity function resulting from the analysis of different data sets.

References

[1] C. Murray and A. J. Orr-Ewing, Int. Rev. Phys. Chem. **23,** 435 (2004).

[2] S. J. Greaves, R. A. Rose, and A. J. Orr-Ewing, Phys. Chem. Chem. Phys., DOI: 10.1039/C001233E (2010).

[3] J. H. Park, Y. S. Lee, J. F. Hershberger, J. M. Hossenlopp, and G. W. Flynn, J. Am. Chem. Soc. **114,** 58 (1992).

[4] S. A. Kandel and R. N. Zare, J. Chem. Phys. **109,** 9719 (1998).

[5] W. R. Simpson, T. P. Rakitzis, S. A. Kandel, T. Lev-On, and R. N. Zare, J. Chem. Phys. **100,** 7938 (1996).

[6] W. R. Simpson, T. P. Rakitzis, S. A. Kandel, A. J. Orr-Ewing, and R. N. Zare, J. Chem. Phys. **103,** 7313 (1995).

[7] W. R. Simpson, A. J. Orr-Ewing, and R. N. Zare, Chem. Phys. Lett. **212,** 163 (1993).

[8] Z. H. Kim, A. J. Alexander, H. A. Bechtel, and R. N. Zare, J. Chem. Phys. **115,** 179 (2001).

[9] Z. H. Kim, H. A. Bechtel, and R. N. Zare, J. Chem. Phys. **117,** 3232 (2002).

[10] H. A. Bechtel, J. P. Camden, D. J. A. Brown, and R. N. Zare, J. Chem. Phys. **120,** 5096 (2004).

[11] Z. H. Kim, H. A. Bechtel, J. P. Camden, and R. N. Zare, J. Chem. Phys. **122,** 084303 (2005).

[12] J. P. Camden, H. A. Bechtel, D. J. A. Brown, and R. N. Zare, J. Chem. Phys. **123,** 134301 (2005).

[13] H. A. Bechtel, Z. H. Kim, J. P. Camden, and R. N. Zare, Mol. Phys. **103,** 1837 (2005).

[14] H. A. Bechtel, J. P. Camden, D. J. A. Brown, M. R. Martin, R. N. Zare, and K. Vodopyanov, Angew. Chem. Int. Ed. **44,** 2382 (2005).

[15] M. R. Martin, D. J. A. Brown, A. S. Chiou, and R. N. Zare, J. Chem. Phys. **126,** 044315 (2007).

[16] S. A. Kandel, T. P. Rakitzis, T. Lev-On, and R. N. Zare, J. Phys. Chem. A **102,** 2270 (1998).

[17] S. A. Kandel, T. P. Rakitzis, T. Lev-On, and R. N. Zare, Chem. Phys. Lett. **265,** 121 (1997).

[18] S. A. Kandel, T. P. Rakitzis, T. Lev-On, and R. N. Zare, J. Chem. Phys. **105,** 7550 (1996).

[19] M. N. R. Ashfold, N. H. Nahler, A. J. Orr-Ewing, O. P. J. Vieuxmaire, R. L. Toomes, T. N. Kitsopoulos, I. A. Garcia, D. A. Chestakov, S. M. Wu, and D. H. Parker, Phys. Chem. Chem. Phys. **8,** 26 (2006).

[20] A. T. J. B. Eppink and D. H. Parker, Rev. Sci. Instrum. **68,** 3477 (1997).

[21] M. J. Bass, M. Brouard, C. Vallance, T. N. Kitsopoulos, P. C. Samartzis, and R. L. Toomes, J. Chem. Phys. **121,** 7175 (2004).

[22] M. J. Bass, M. Brouard, C. Vallance, T. N. Kitsopoulos, P. C. Samartzis, and R. L. Toomes, J. Chem. Phys. **119,** 7168 (2003).

[23] R. L. Toomes, A. J. van den Brom, T. N. Kitsopoulos, C. Murray, and A. J. Orr-Ewing, J. Phys. Chem. A **108,** 7909 (2004).

[24] C. Murray, A. J. Orr-Ewing, R. L. Toomes, and T. N. Kitsopoulos, J. Chem. Phys. **120,** 2230 (2004).

[25] R. L. Toomes and T. N. Kitsopoulos, Phys. Chem. Chem. Phys. **5,** 2481 (2003).

[26] W. Li, C. S. Huang, M. Patel, D. Wilson, and A. Suits, J. Chem. Phys. **124,** 011102 (2006).

27   C. S. Huang, W. Li, and A. G. Suits, J. Chem. Phys. **125,** 133107 (2006).

28   M. Ahmed, D. S. Peterka, and A. G. Suits, Chem. Phys. Lett. **317,** 264 (2000).

29   B. Retail, J. K. Pearce, C. Murray, and A. J. Orr-Ewing, J. Chem. Phys. **122,** 101101 (2005).

30   J. K. Pearce, B. Retail, S. J. Greaves, R. A. Rose, and A. J. Orr-Ewing, J. Phys. Chem. A **111,** 13296 (2007).

31   B. Retail, S. J. Greaves, J. K. Pearce, R. A. Rose, and A. J. Orr-Ewing, Phys. Chem. Chem. Phys. **9,** 3261 (2007).

32   R. A. Rose, S. J. Greaves, and A. J. Orr-Ewing, Mol. Phys.**,** in press (2010).

33   H. Kawamata, S. Tauro, and K. Liu, Phys. Chem. Chem. Phys. **10,** 4378 (2008).

34   S. Yan, Y. T. Wu, B. L. Zhang, X. F. Yue, and K. P. Liu, Science **316,** 1723 (2007).

35   Z. H. Kim, H. A. Bechtel, and R. N. Zare, J. Am. Chem. Soc. **123,** 12714 (2001).

36   F. F. Crim, Proc. Nat. Acad. Sci. U.S.A **105,** 12654 (2008).

37   C. J. Annesley, A. E. Berke, and F. F. Crim, J. Phys. Chem. A **112,** 9448 (2008).

38   R. J. Holiday, C. H. Kwon, C. J. Annesley, and F. F. Crim, J. Chem. Phys. **125,** 133101 (2006).

39   S. Yoon, R. J. Holiday, E. L. Sibert, and F. F. Crim, J. Chem. Phys. **119,** 9568 (2003).

40   S. Yoon, S. Henton, A. N. Zivkovic, and F. F. Crim, J. Chem. Phys. **116,** 10744 (2002).

41   B. Retail, J. K. Pearce, S. J. Greaves, R. A. Rose, and A. J. Orr-Ewing, J. Chem. Phys. **128,** 184303 (2008).

42   J. G. Zhou, J. J. Lin, B. L. Zhang, and K. P. Liu, J. Phys. Chem. A **108,** 7832 (2004).

43   B. Zhang and K. Liu, J. Chem. Phys. **122,** 101102 (2005).

44   S. Rudić, C. Murray, D. Ascenzi, H. Anderson, J. N. Harvey, and A. J. Orr-Ewing, J. Chem. Phys. **117,** 5692 (2002).

45   S. Rudić, D. Ascenzi, and A. J. Orr-Ewing, Chem. Phys. Lett. **332,** 487 (2000).

46   S. Rudić, C. Murray, J. N. Harvey, and A. J. Orr-Ewing, Phys. Chem. Chem. Phys **5,** 1205 (2003).

47   C. Murray, B. Retail, and A. J. Orr-Ewing, J. Chem. Phys. **301,** 239 (2004).

48   J. K. Pearce, C. Murray, and A. J. Orr-Ewing, Phys. Scripta **73,** C14-C19 (2006).

49   J. K. Pearce, PhD Thesis, University of Bristol, 2007.

50   C. Murray, J. K. Pearce, S. Rudić, B. Retail, and A. J. Orr-Ewing, J. Phys. Chem. A **109,** 11093 (2005).

51   C. G. Elles and F. F. Crim, Ann. Rev. Phys. Chem. **57,** 273 (2006).

52   L. Sheps, A. C. Crowther, S. L. Carrier, and F. F. Crim, J. Phys. Chem. A **110,** 3087 (2006).

53   L. Sheps, A. C. Crowther, C. G. Elles, and F. F. Crim, J. Phys. Chem. A **109,** 4296 (2005).

54   F. J. Aoiz, M. Brouard, P. A. Enriquez, and R. Sayos, J. Chem. Soc. Faraday Trans. **89,** 1427 (1993).

55   N. E. Shafer, A. J. Orr-Ewing, W. R. Simpson, H. Xu, and R. N. Zare, Chem. Phys. Lett. **212,** 155 (1993).

56   L. Schnieder, K. Seekamp-Rahn, E. Wrede, and K. H. Welge, J. Chem. Phys. **107,** 6175 (1997).

57   S. Rudić, C. Murray, J. N. Harvey, and A. J. Orr-Ewing, J. Chem. Phys. **120,** 186 (2004).

58   A. J. Orr-Ewing, W. R. Simpson, T. P. Rakitzis, S. A. Kandel, and R. N. Zare, J. Chem. Phys. **106,** 5961 (1997).

59   S. J. Greaves, A. J. Orr-Ewing, and D. Troya, J. Phys. Chem. A **112,** 9387 (2008).

60   S. J. Greaves, J. Kim, A. J. Orr-Ewing, and D. Troya, Chem. Phys. Lett. **441,** 171 (2007).

61   A. Fernandez-Ramos, E. Martinez-Nunez, J. M. C. Marques, and S. A. Vazquez, J. Chem. Phys. **118,** 6280 (2003).

62   D. F. Varley and P. J. Dagdigian, J. Phys. Chem. **99,** 9843 (1995).

63   D. A. Blank, N. Hemmi, A. G. Suits, and Y. T. Lee, Chem. Phys. **231,** 261 (1998).

64   Y. F. Yen, Z. R. Wang, B. Xue, and B. Koplitz, J. Phys. Chem. **98,** 4 (1994).

65   J. H. Knox and R. L. Nelson, Trans. Faraday Soc. **55,** 937 (1959).

66   H. O. Pritchard, J. B. Pyke, and A. F. Trotmandickenson, J. Am. Chem. Soc. **77,** 2629 (1955).

67   D. M. Rowley, R. Lesclaux, P. D. Lightfoot, K. Hughes, M. D. Hurley, S. Rudy, and T. J. Wallington, J. Phys. Chem. **96,** 7043 (1992).

68   R. Atkinson and S. M. Aschmann, Int. J. Chem. Kinet. **17,** 33 (1985).

69   K. G. Kambanis, Y. G. Lazarou, and P. Papagiannakopoulos, Int. J. Chem. Kinet. **27,** 343 (1995).

70   Y. G. Lazarou and P. Papagiannakopoulos, J. Phys. Chem. **97,** 6806 (1993).

71   R. Walsh, Acc. Chem. Res. **14,** 246 (1981).

72   P. M. Regan, S. R. Langford, D. Ascenzi, P. A. Cook, A. J. Orr-Ewing, and M. N. R. Ashfold, Phys. Chem. Chem. Phys. **1,** 3247 (1999).

73   J. D. D. Martin and J. W. Hepburn, J. Chem. Phys. **109,** 8139 (1998).

74   D. F. McMillen and D. M. Golden, Ann. Rev. Phys. Chem. **33,** 493 (1982).

75   D. L. Baulch, C. T. Bowman, C. J. Cobos, R. A. Cox, T. Just, J. A. Kerr, M. J. Pilling, D. Stocker, J. Troe, W. Tsang, R. W. Walker, and J. Warnatz, J. Phys. Chem. Ref. data **34,** 757 (2005).

76   S. P. Sander, R. R. Friedl, D. M. Golden, M. J. Kurylo, G. K. Moortgat, H. Keller-Rudek, P. H. Wine, A. R. Ravishankara, C. E. Kolb, M. J. Molina, B. J. Finlayson-Pitts, R. E. Huie, and V. L. Orkin, *Chemical Kinetics and Photochemical Data for use in Atmospheric Studies: Evaluation Number 15* (Jet Propulsion Laboratory, California Institute of Technology, Pasadena CA, 2006).

77   H. Qian, D. Turton, P. W. Seakins, and M. J. Pilling, Int. J. Chem. Kinet. **34,** 86 (2001).

78   B. Retail, R. A. Rose, J. K. Pearce, S. J. Greaves, and A. J. Orr-Ewing, Phys. Chem. Chem. Phys. **10,** 1675 (2008).

79   A. D. Estillore, L. M. Visger, and A. G. Suits, J. Chem. Phys. **132,** 164313 (2010).

80   X. H. Liu, R. L. Gross, G. E. Hall, J. T. Muckerman, and A. G. Suits, J. Chem. Phys. **117,** 7947 (2002).

81   M. J. Frisch, G. W. Trucks, H. B. Schlegel, G. E. Scuseria, M. A. Robb, J. R. Cheeseman, J. J. A. Montgomery, T. Vreven, K. N. Kudin, J. C. Burant, J. M. Millam, S. S. Iyengar, J. Tomasi, V. Barone, B. Mennucci, M. Cossi, G.

Scalmani, N. Rega, G. A. Petersson, H. Nakatsuji, M. Hada, M. Ehara, K. Toyota, R. Fukuda, J. Hasegawa, M. Ishida, T. Nakajima, Y. Honda, O. Kitao, H. Nakai, M. Klene, X. Li, J. E. Knox, H. P. Hratchian, J. B. Cross, V. Bakken, C. Adamo, J. Jaramillo, R. Gomperts, R. E. Stratmann, O. Yazyev, A. J. Austin, R. Cammi, C. Pomelli, J. Ochterski, P. Y. Ayala, K. Morokuma, G. A. Voth, P. Salvador, J. J. Dannenberg, V. G. Zakrzewski, S. Dapprich, A. D. Daniels, M. C. Strain, O. Farkas, D. K. Malick, A. D. Rabuck, K. Raghavachari, J. B. Foresman, J. V. Ortiz, Q. Cui, A. G. Baboul, S. Clifford, J. Cioslowski, B. B. Stefanov, G. Liu, A. Liashenko, P. Piskorz, I. Komaromi, R. L. Martin, D. J. Fox, T. Keith, M. A. Al-Laham, C. Y. Peng, A. Nanayakkara, M. Challacombe, P. M. W. Gill, B. G. Johnson, W. Chen, M. W. Wong, C. Gonzalez, and J. A. Pople, *GAUSSIAN 03 (Revision D.01),* (Wallingford, CT, 2004).

[82]   C. A. Picconatto, A. Srivastava, and J. J. Valentini, J. Chem. Phys. **114,** 1663 (2001).

[83]   J. C. Polanyi, Acc. Chem. Res. **5,** 161 (1972).

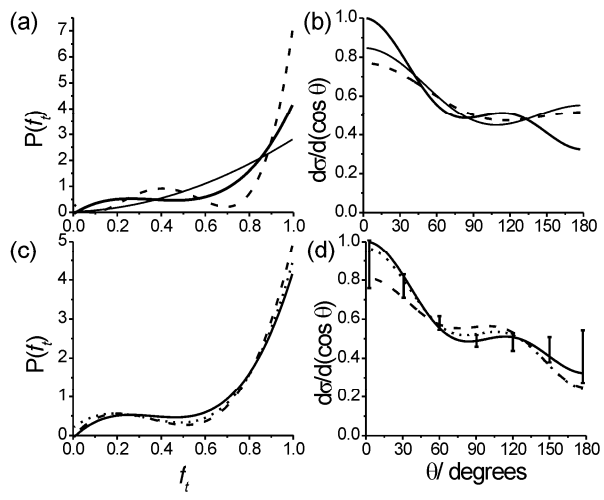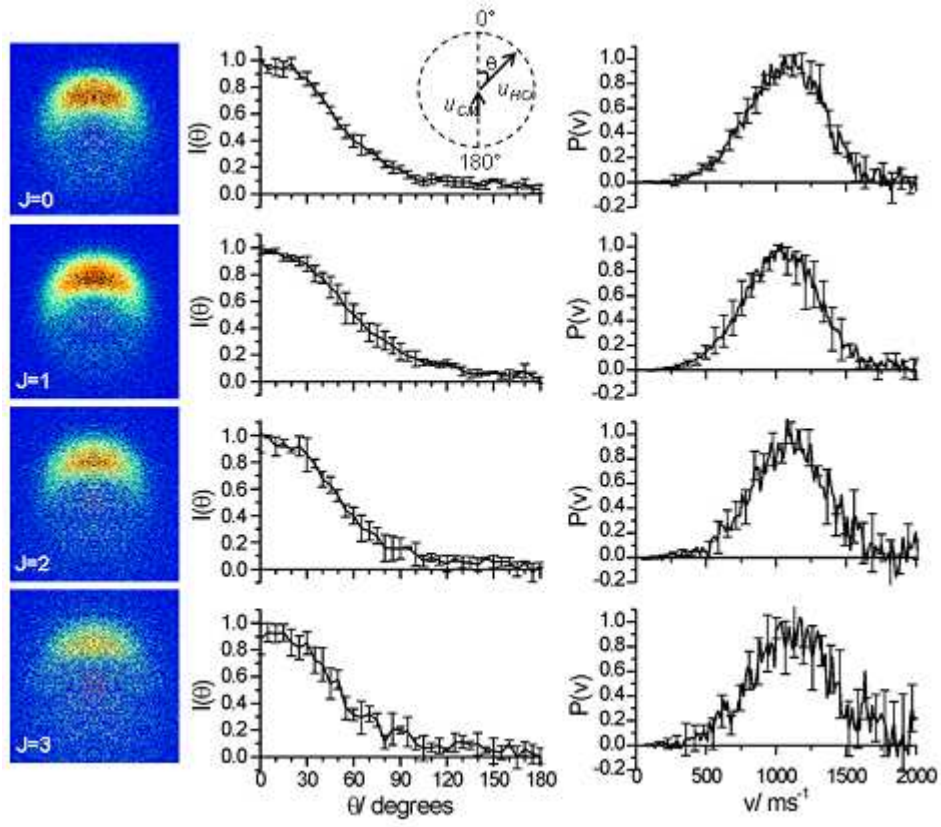[84]   R. D. Levine, *Molecular Reaction Dynamics* (Cambridge University Press, 2005).
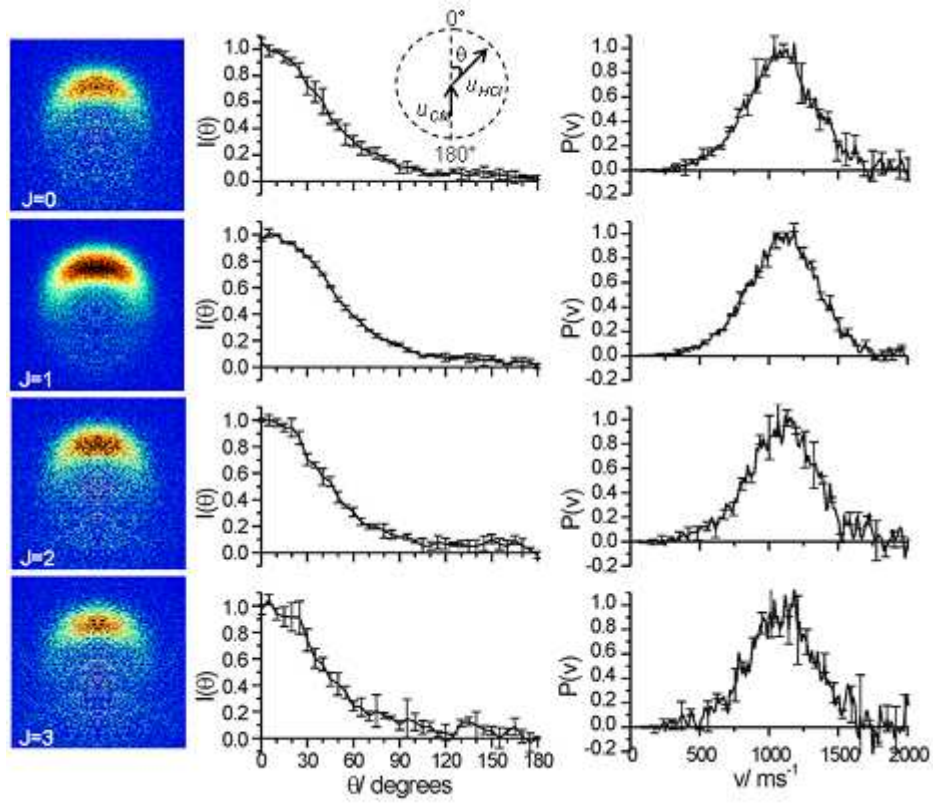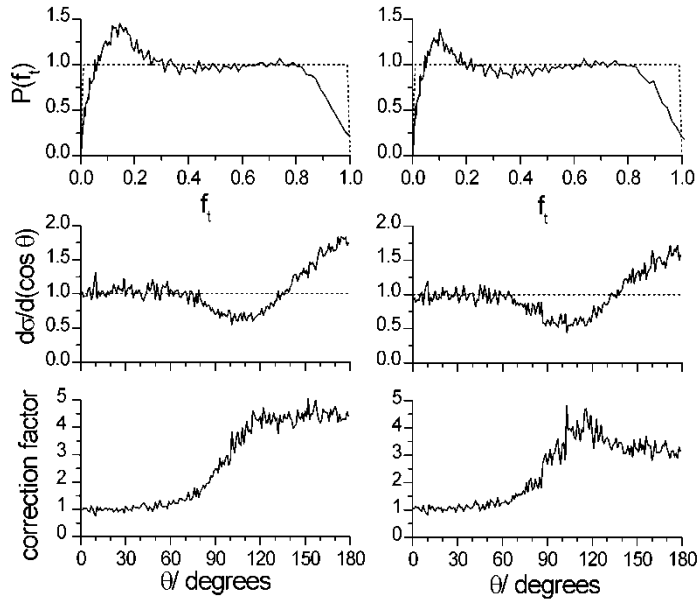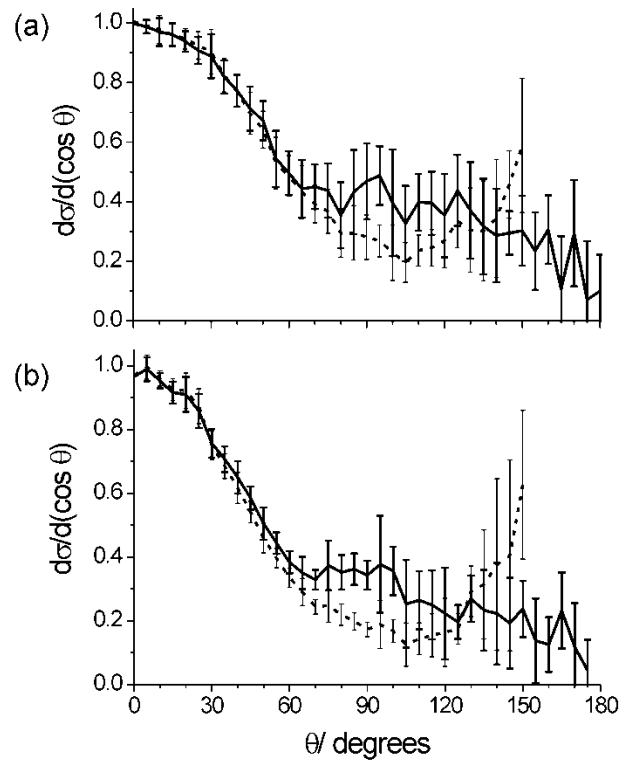
Figure 1
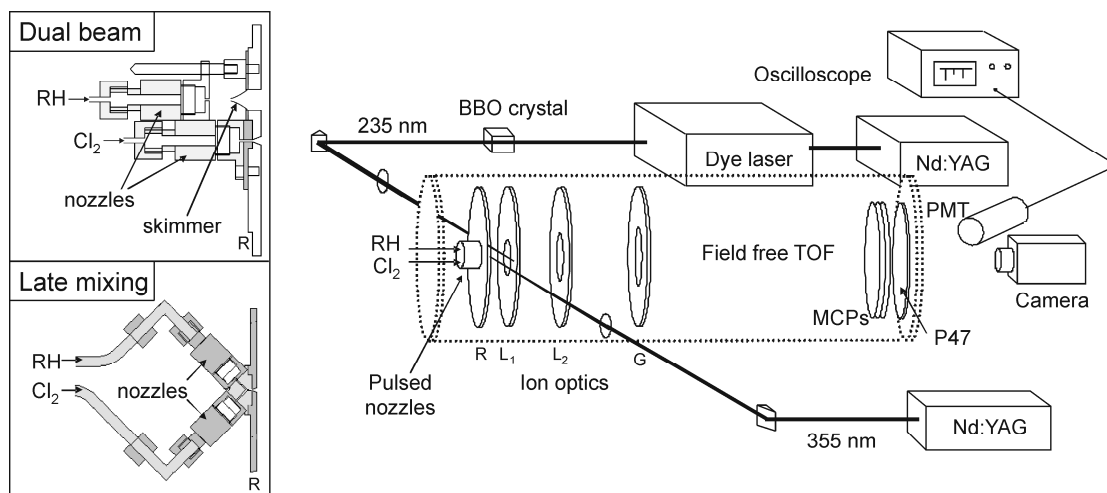
Figure 2
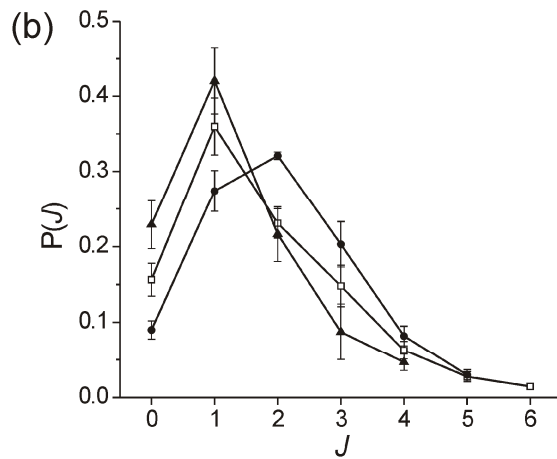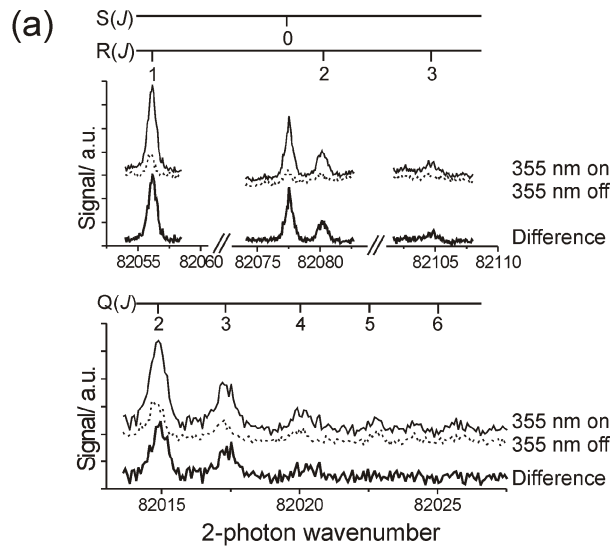
Figure 3
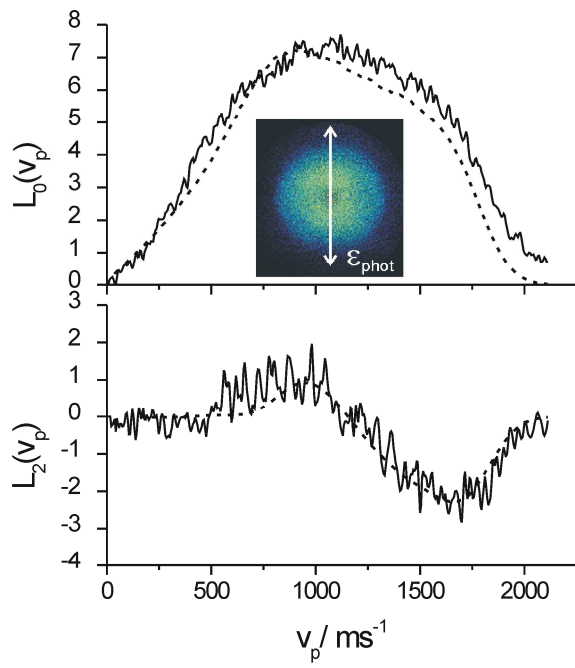
Figure 4

Figure 5

Figure 6

Figure 7

Figure 8

Figure 9

Figure 10

Figure 11

(a)

(b)

b/b$_{max}$